CORE
Metadata, citation and similar papers at core.ac.uk
Provided by Institutional Repository of the Freie Universität Berlin

Fluence-dependent dynamics of the 5d6s exchange splitting in Gd metal after femtosecond laser excitation

Björn Frietsch[1,2]*, Robert Carley[1,2], Markus Gleich[1], Martin Teichmann[1,2], John Bowlan[1], and Martin Weinelt[1]*

[1]*Department of Physics, Freie Universität Berlin, 14195 Berlin, Germany*

[2]*Max-Born-Institut, 12489 Berlin, Germany*

E-mail: b.frietsch@fu-berlin.de, weinelt@physik.fu-berlin.de

We investigate the fluence-dependent dynamics of the exchange-split 5d6s valence bands of Gd metal after femtosecond, near-infrared (IR) laser excitation. Time- and angle-resolved photoelectron spectroscopy (tr-ARPES) with extreme ultraviolet (XUV) probe pulses is used to simultaneously map the transient binding energies of the minority and majority spin valence bands. The decay constant of the exchange splitting increases with fluence. This reflects the slower response of the occupied majority-spin component, which we attribute to Elliot-Yafet spin-flip scattering in accordance with the microscopic three-temperature model (M3TM). In contrast, the time constant of the partly unoccupied minority-spin band stays unaffected by a change in pump fluence. Here, we introduce as an alternative to superdiffusive spin transport exchange scattering, which is an ultrafast electronic mechanism explaining the observed dynamics. Exchange scattering can reduce the spin polarization in the partially unoccupied minority-spin band and thus its energetic position without effective demagnetization.

1. Introduction

Gadolinium is commonly regarded as a model system for the Heisenberg ferromagnet. The half-filled 4f shell gives rise to a large spin moment of $S_{4f} = 7\ \mu_B$ per atom. The direct exchange between the 4f electrons of neighboring atoms is negligible because of the localized character of the Gd 4f orbitals[1)]. Ferromagnetic ordering is established by an indirect exchange (Ruderman-Kittel-Kasuya-Yosida) interaction via the hybridized, itinerant $(5d6s)^3$ valence electrons. These spin-polarized valence electrons contribute an additional $0.63\ \mu_B$ per atom to the overall magnetic moment[2)]. At 90 K, the minority and majority spin components of the valence band are separated by an exchange splitting of

about 0.9 eV [3] and exhibit a spin polarization of about 70-80% [4]. We use changes in this splitting as a probe for the magnetization dynamics. The exact relationship between the spin polarization and the exchange splitting is not known for nonthermal dynamics[5] and its behavior above the Curie temperature still remains a controversial topic[4,6].

The ultrafast magnetization dynamics of Gd metal have been investigated extensively in recent years. Results from a wide variety of experimental[5-13] and theoretical[14-20] approaches have been reported, but to date no consensus on the underlying processes has been achieved. Here, we will focus on the microscopic mechanisms responsible for the fluence-dependent dynamics of the itinerant 5d6s electrons after laser excitation, and compare our results of tr-ARPES with calculations obtained using a modified M3TM[14].

2. Experimental methods

We performed measurements on a 10 nm-thick Gd(0001) film grown epitaxially on a W(110) substrate (see Refs. 7 and 21 for sample preparation details). The experimental setup was based on a commercial Ti:sapphire laser that delivers 40 fs IR pump pulses at 790 nm with a repetition rate of 10 kHz. The high-order harmonic generation of the IR yielded XUV probe pulses. We used the 23rd harmonic at 36 eV to probe the sample at the Γ-point in the fourth Brillouin zone. The photon energy was selected by a toroidal-grating monochromator with an energy resolution of 100 meV. The XUV pulse duration was a 100 fs full-width at half-maximum (FWHM). The total time resolution of the measurement was determined by the pump pulse, stretched to 300 fs (FWHM) in order to minimize IR-induced space charge effects, which are prominent for the Gd(0001) surface owing to its low work function of 3.7 eV [22]. Further details of the experimental apparatus can be found in Ref. 21.

Figure 1 shows a typical ARPES measurement for ferromagnetic Gd recorded at 90 K. With increasing binding energy, we observe the surface state, the exchange-split 5d6s valence bands, and the 4f level. The magnetization dynamics of the surface state and the 4f levels have recently been reported (Refs. 5 and 9, respectively). To follow the dynamics of the exchange-split valence bands, we integrate a small angular slice of the photoelectron spectra around the Γ-point and determine the binding energies of the different states by fitting. For the analysis of the data obtained in pump-probe experiments, we include the position of the 4f state to determine the Fermi energy. In this manner, we can correct for pump

pulse-induced space-charge effects that can lead to shifts in the spectra, since the thermal shift of the 4f binding energy is negligible[7,23]. The spectral line shapes of the states are given by Cauchy-Lorentz distributions with the intrinsic linewidth determined by the photohole lifetime. For the fit of the Gd spectrum in Fig. 1, we use 5 different Lorentzians describing the sharp surface-state peak (not shown), the minority (red) and majority (blue) components of the 5d6s valence band, and the 4f state (gray), which is represented by a combination of two Lorenzians. In reality, the 4f state consists of an unresolvable multiplet of 7 components, with a second set of components separated by the surface core level shift of about 0.48 eV [24]. The fit by two Lorentzians is therefore only a rough approximation, which is sufficient in our case since we are only interested in the 4f energetic position to adjust the Fermi level.

Because we have no special spin-dependent selection rules in our photoemission experiment, the intensities of the minority and majority valence band components are set to be the same. The difference in spectral width accounts for the lifetime of the photohole, which decreases with increasing binding energy, i.e., the different number of electrons available for filling the corresponding photohole. The width of the surface state at negative time delays mainly reflects our energy resolution of about 140 meV. Measurements with high energy resolution revealed an intrinsic width of only 70 meV FWHM for the surface state at 90 K [25]. Such a width is increased during the excited phase of the electronic system as the hot electrons above the Fermi level decrease the lifetime of the surface state photohole. All bulk states contribute to a Shirley background to account for the scattering probability of the electrons on their way to the surface. This background is proportional to the energy-integrated peak intensities starting at the Fermi level. In addition to this, a linear background must be introduced to characterize the spectrum fully. It rises towards the Fermi level and defines the contribution of phonon-scattered electrons coming from other k-points, reflecting the increasing density of states [3,26].

Finally, to obtain a complete energy distribution curve, all spectral features are cut by the Fermi edge and convolved with a Gaussian to account for the experimental resolution determined by the XUV monochromator and hemispherical analyzer[21]. For maximum objectivity and consistency, all spectra in a pump-probe dataset were fitted using the same starting parameter and identical boundary conditions.

3. Results and discussion

Changes in the binding energies of the minority and majority spin valence bands following laser excitation are shown for two different pump fluences in Fig. 2. Most notably, the bands do not move simultaneously, as expected from static, temperature-dependent measurements[3]. Instead, we find an initial response of the minority valence band for both pump fluences that is too fast to be resolved by our time resolution of 0.3 ps. The response of the majority band, on the other hand, is delayed by about half a picosecond and exhibits much slower time constants that vary with the pump fluence: 0.8 ±0.1 ps and 1.4 ±0.2 ps for pump fluences of 3.1 and 4.6 mJ/cm^2, respectively. Because of these different and fluence-dependent time constants, we conclude that different processes are responsible for the individual dynamics of the minority and majority spin bands. This is a startling result since they originate from the same 5d6s band. The slight delay in the majority band between the two fluences, as suggested by the exponential fit, is within the error bars.

It is well known that the femtosecond-laser excitation of metals generates an initial nonequilibrium electronic state that thermalizes on the timescale of around 100 fs to produce a hot electron gas characterized by an electronic temperature T_e [27-30]. The excited electrons scatter with phonons, leading to lattice heating in the first 1-2 picoseconds. Comparing these timescales with the observed dynamics, we attribute the fast response of the minority band to exchange scattering between hot electrons of opposite spins[31]. This process is ultrafast owing to the high energy of the excited electrons and establishes a defined electron temperature after laser excitation[13]. Thereby, the overall magnetization of the sample would not change, but the polarization of the partially occupied minority valence band can be reduced by spin mixing through the admission of excited majority electrons. Varying the fluence seems to only affect the amplitude of the minority band shift. We note that in addition to the discussed exchange scattering of hot electrons, the superdiffusive spin-dependent transport[15] of hot electrons between the surface and the bulk can contribute to the observed ultrafast response of the minority spin band[8].

In contrast to the fast minority response, the slower majority correlates with lattice heating, which is limited to timescales set by the most energetic phonon branches of about 15 meV [32]. It seems that this slower phononic response also affects the minority band and leads to a minor relaxation back towards lower binding energies. In combination, the dynamics of the minority and the majority spin bands reduces the exchange splitting whereby the amplitude

of the reduction is given by the shift of both. However, it is only the fluence dependence of the time constant of the fully occupied majority spin band that gives rise to the fluence dependence of the time constant of the exchange splitting. Fluence-dependent demagnetization rates were previously seen in magneto-optical Kerr effect measurements (MOKE) of Gd[10] and Ni[33,34]. For Ni, they were explained by the microscopic three-temperature model (M3TM)[14]. The M3TM is based on Elliott-Yafet phonon-magnon scattering and connects the lattice dynamics to the spin dynamics and thus to the magnetization dynamics.

Figure 3 shows the magnetization dynamics as predicted by a slightly modified M3TM. The M3TM introduced by Koopmans *et al.*[14] in 2010 extends the two-temperature model (2TM) of Anisimov *et al.*[35] by the magnetic system using a mean-field Weiss approach and includes Elliott-Yafet spin-flip scattering[36,37] as the microscopic origin of the magnetization dynamics. In our simulations, we modified the M3TM to include the laser excitation process, i.e., in analogy to earlier studies,[38,39] a source term is added to the equation of the electron temperature T_e. Beside this, we used the temperature dependence of the electronic heat capacity $C_e = C_{e,0} \cdot T_e$, as already performed in other 2TM calculations[30,39]. This plays a significant role directly after laser excitation where T_e reaches values of several thousand Kelvin. To simulate the effect of the substrate, which acts as a heat sink, we assumed a 1000-nm-thick Gd sample, where the electron temperature T_e at its back is set to be low at all times. We further assumed that no heat transport through the surface (vacuum interface) occurs. In addition, the following physical constants were used for the simulations (in SI units): the phonon heat capacity $C_p = 1.51 \times 10^6 \frac{J}{m^3 K}$ (Ref. [40]), the energy exchange rate between the electron and phonon systems $g = 0.25 \times 10^{18} \frac{J}{s m^3 K}$ (Ref. [30]), the Curie temperature $T_C = 292.5\,\mathrm{K}$ (Ref. 41), the electronic heat capacity $C_e = C_{e,0}\, T_e$ with $C_{e,0} = 225\ \frac{J}{m^3 K^2}$ (Ref. 30), and the material-specific constant $R = 0.092\,\mathrm{ps}^{-1}$ (Ref. 14). Following the work of Hohlfeld *et al.*[42] and Bovensiepen,[30] we used an effective optical penetration depth of $\lambda = 40\,\mathrm{nm}$ to account for ballistic electron transport. The calculations were performed with a constant electronic thermal conductivity, as in the case of the unmodified M3TM. To reflect the actual temperature dependence of the electronic thermal conductivity $K_e = K_{e,0} T_e / T_p$, we assumed an increased value of $K_e = 110 \frac{J}{s m K}$, which is reasonable shortly after laser excitation, when the electron temperature exceeds the phonon temperature significantly[43].

The simulations in Fig. 3 show the predicted temperatures and magnetizations at the sample surface for the two absorbed fluences of 3.1 and 4.6 mJ/cm² used in the above measurements. As expected, we find that, for higher excitation densities, electron and phonon subsystems equilibrate at later delays. The slightly higher lattice temperature at delays of 2-3 ps reflects the ongoing electronic heat transport into the bulk. A single exponential fit to the calculated magnetization shown in Fig. 3(b) reflects the time constants found in the measured collapse of the exchange splitting. This corroborates that Elliott-Yafet scattering, which depends on electron and phonon temperatures, determines the response of the majority spin band and thus the exchange splitting. However, a quantitative comparison of the model with the experiment must be regarded with caution since the M3TM oversimplifies the magnetic system of Gd by choosing a mean-field Weiss approach. The latter does not distinguish between localized 4f and itinerant 5d6s electrons, which show a disparate response after laser excitation[9]. The initially disjoint 4f magnetic moments are also the reason for the observed difference in demagnetization amplitude between the probed 5d6s bands and the simulation results in the present study. In addition, dynamic parameters such as the electronic thermal conductivity are set constant in the simulation and important effects such as spin-orbit coupling are not included but might have a strong influence[8]. Nevertheless, the fluence dependence of the time constant that we find in the simulation is induced in the experiment by the majority valence band movement, so the Elliott-Yafet-like spin-flip scattering, which drives the dynamics of the M3TM, is likely the process responsible for the majority band dynamics.

4. Conclusions

This work has revealed microscopic details of the ultrafast laser-driven magnetization dynamics of the valence bands of ferromagnetic Gd. We have observed different fluence-dependent behaviors between the majority and minority spin components of the valence band following excitation by a 300 fs laser pulse. This provides evidence for both pure electronic scattering and phonon-mediated spin-flip scattering (Elliott-Yafet scattering) during ultrafast demagnetization. The fast response of the minority spin band is disentangled from the electron-phonon equilibration time, suggesting exchange scattering of hot electrons as the origin of its shift. The fluence dependence of the slower majority response is qualitatively in line with dynamics caused by an electron-phonon-mediated spin-flip scattering as proposed by the M3TM.

These results raise the question of how the observed nonequilibrium between the minority and majority spin bands is maintained for the first few picoseconds after excitation and how it is finally dissipated.

Acknowledgments

We gratefully acknowledge funding from the Leibniz Graduate School *Dynamics in New Light*, the Helmholtz Virtual Institute *Dynamic Pathways in Multidimensional Landscapes* and the Deutsche Forschungsgemeinschaft through grant WE2037/4-1. JB is indebted to the Humboldt Foundation for a postdoctoral fellowship.

References

1) B. N. Harmon and A. J. Freeman, Phys. Rev. B **10**, 1979 (1974).
2) L. W. Roeland, G. J. Cock, F. A. Muller, A. C. Moleman, K. A. McEwen, R. G. Jordan, and D. W. Jones, J. Phys. F: Met. Phys. **5**, L233 (1975).
3) C. Schüßler-Langeheine, PhD thesis, Freie Universität Berlin (1999).
4) K. Maiti, M. C. Malagoli, A. Dallmeyer, and C. Carbone, Phys. Rev. Lett. **88**, 167205 (2002).
5) B. Andres, M. Christ, C. Gahl, M. Wietstruk, M. Weinelt, and J. Kirschner, Phys. Rev. Lett. **115**, 207404 (2015).
6) B. Frietsch, J. Bowlan, R. Carley, M. Teichmann, J. Wolter, and M. Weinelt, Springer Proc. Phys. **159**, 274 (2015).
7) R. Carley, K. Döbrich, B. Frietsch, C. Gahl, M. Teichmann, O. Schwarzkopf, P. Wernet, and M.Weinelt, Phys. Rev. Lett. **109**, 057401 (2012).
8) M. Teichmann, B. Frietsch, K. Döbrich, R. Carley, and M.Weinelt, Phys. Rev. B **91**, 014425 (2015).
9) B. Frietsch, J. Bowlan, R. Carley, M. Teichmann, S. Wienholdt, D. Hinzke, U. Nowak, K. Carva, P. M. Oppeneer, and M. Weinelt, Nat. Comm. **6**, 8262 (2015).
10) M. Sultan, A. Melnikov, and U. Bovensiepen, Phys. Status Solidi B **248**, 2323 (2011).
11) M. Wietstruk, A. Melnikov, C. Stamm, T. Kachel, N. Pontius, M. Sultan, C. Gahl, M. Weinelt, Hermann A. Dürr, and Uwe Bovensiepen, Phys. Rev. Lett. **106**, 127401 (2011).
12) A. Melnikov, H. Prima-Garcia, M. Lisowski, T. Gießel, R. Weber, R. Schmidt, C. Gahl, N. M. Bulgakova, U. Bovensiepen, and M. Weinelt, Phys. Rev. Lett. **100**, 107202 (2008).
13) M. Lisowski, P. A. Loukakos, A. Melnikov, I. Radu, L. Ungureanu, M. Wolf, and U. Bovensiepen, Phys. Rev. Lett. **95**, 137402 (2005).
14) B. Koopmans, G. Malinowski, F. Dalla Longa, D. Steiauf, M. Fähnle, T. Roth, M. Cinchetti, and M. Aeschlimann. Nat. Mater. **9**, 259 (2010).
15) M. Battiato, K. Carva, and P. M. Oppeneer, Phys. Rev. Lett. **105**, 027203 (2010).
16) U. Atxitia and O. Chubykalo-Fesenko, Phys. Rev. B **84**, 144414 (2011).
17) S. Essert and H.C. Schneider, Phys. Rev. B **84**, 224405 (2011).
18) M. Fähnle and C. Illg, J. Phys.: Condens. Matter **23**, 493201 (2011).
19) S. Wienholdt, D. Hinzke, K. Carva, P. M. Oppeneer, and U. Nowak, Phys. Rev. B **88**, 020406(R) (2013).
20) B. Y. Mueller and B. Rethfeld, Phys. Rev. B **90**, 144420 (2014).
21) B. Frietsch, R. Carley, K. Döbrich, C. Gahl, M. Teichmann, O. Schwarzkopf, P. Wernet and M. Weinelt, Rev. Sci. Inst. **84**, 075106 (2013).
22) B. Andres, Diploma Thesis, Freie Universität Berlin, (2010).
23) B. Frietsch, PhD Thesis, Freie Universität Berlin (2015).
24) F. Gerken, J. Barth, and R. Kammerer, Surf. Sci. **117**, 468 (1982).
25) A. Melnikov, I. Radu, U. Bovensiepen, O. Krupin, K. Starke, E. Matthias, and M. Wolf, Phys. Rev. Lett. **91**, 227403 (2003).
26) R. C. White, C. S. Fadley, M. Sagurton, P. Roubin, D. Chandesris, J. Lecante, C. Guillot, and Z. Hussain, Phys. Rev. B **35**, 1147 (1987).
27) W. S. Fann, R. Storz, H. W. K. Tom, and J. Bokor, Phys. Rev. B **46**, 13592 (1992).
28) H.-S. Rhie, H. A. Dürr, and W. Eberhardt, Phys. Rev. Lett. **90**, 247201 (2003).
29) M. Lisowski , P.A. Loukakos, U. Bovensiepen, J. Stähler, C. Gahl, and M. Wolf, Appl. Phys. A **78**, 165 (2004).
30) U. Bovensiepen, J. Phys.: Condens. Matter **19**, 083201 (2007).
31) A. V. Fedorov, T. Valla, F. Liu, P. D. Johnson, M. Weinert, and P. B. Allen, Phys. Rev. B **65**, 212409 (2002).
32) S. S. Kushwaha and A. Kumar, J. Phys. C **4**, 1674 (1971).
33) J. Hohlfeld, E. Matthias, R. Knorren, and K. H. Bennemann, Phys. Rev. Lett. **78**, 4861 (1997).
34) T. Roth, A. J. Schellekens, S. Alebrand, O. Schmitt, D. Steil, B. Koopmans, M. Cinchetti, and M. Aeschlimann, Phys. Rev. X **2**, 021006 (2012).
35) S. I. Anisimov, B. L. Kapeliovich, and T. L. Perelman, Zh. Eksp. Teor. Fiz **66**, 375 (1974).
36) R. J. Elliott, Phys. Rev. **96**, 266 (1954).
37) Y. Yafet, Solid State Phys. **14** (1963).
38) S.-S. Wellershoff, J. Hohlfeld, J. Güdde, and E. Matthias, Appl. Phys. A **69**, 99 (1999).
39) Y. P. Meshcheryakov and N. M. Bulgakova, Appl. Phys. A **82**, 363 (2005).
40) S. Y. Dan'kov, A. M. Tishin, V. K. Pecharsky, and K. A. Gschneidner, Phys. Rev. B **57**, 3478 (1998).

41) M. Farle, K. Baberschke, U. Stetter, A. Aspelmeier, and F. Gerhardter, Phys. Rev. B **47**, 11571(R) (1993).
42) J. Hohlfeld, S.-S. Wellershoff, J. Güdde, U. Conrad, V. Jähnke, and E. Matthias, Chem. Phys. **251**, 237 (2000).
43) A. P. Kanavin, I. V. Smetanin, V. A. Isakov, Yu. V. Afanasiev, B. N. Chichkov, B. Wellegehausen, S. Nolte, C. Momma, and A. Tünnermann, Phys. Rev. B **57**, 14698 (1998).

Figure Captions

Fig. 1. Inset: ARPES spectrum of a 10-nm-thick ferromagnetic Gd(0001) film at 90 K. A selected energy distribution curve from the highlighted area ±0.15Å^{-1} around the Γ-point was fitted with the spectral components depicted below the experimental curve. Fitting gives the gray line that closely reproduces the experimental data. The binding energy of the minority and majority bands is extracted as a function of pump-probe delay to follow their evolution after laser excitation (see Fig. 2).

Fig. 2. (a) Comparison of the Gd 5d6s valence band dynamics for absorbed pump fluences of 3.1 (gray squares) and 4.6 mJ/cm^2 (black squares). Solid lines are single exponential fits that yield the displayed time constants. The top panel shows the minority component of the exchange-split 5d6s bands which exhibits a time constant reflecting the stretched pump-pulse length of 0.3 ps. The response of its majority spin counterpart, depicted in the bottom panel, is delayed and shows fluence-dependent time constants of 0.8 and 1.4 ps. (b) Dynamics of the corresponding exchange splittings.

Fig. 3. Simulations with the modified M3TM for the two measured pump fluences. The excitation was modeled for a 300 fs, 800 nm laser pulse. (a) Electron (T_e) and phonon (T_p) temperatures as a function of pump-probe delay. For the increased excitation density, the time at which the electron and lattice temperatures converge shifts to later delays. (b) Corresponding magnetization dynamics. The calculation shows a fluence-dependent demagnetization time constant, which is in line with the behavior of the exchange splitting induced by the majority valence band dynamics.

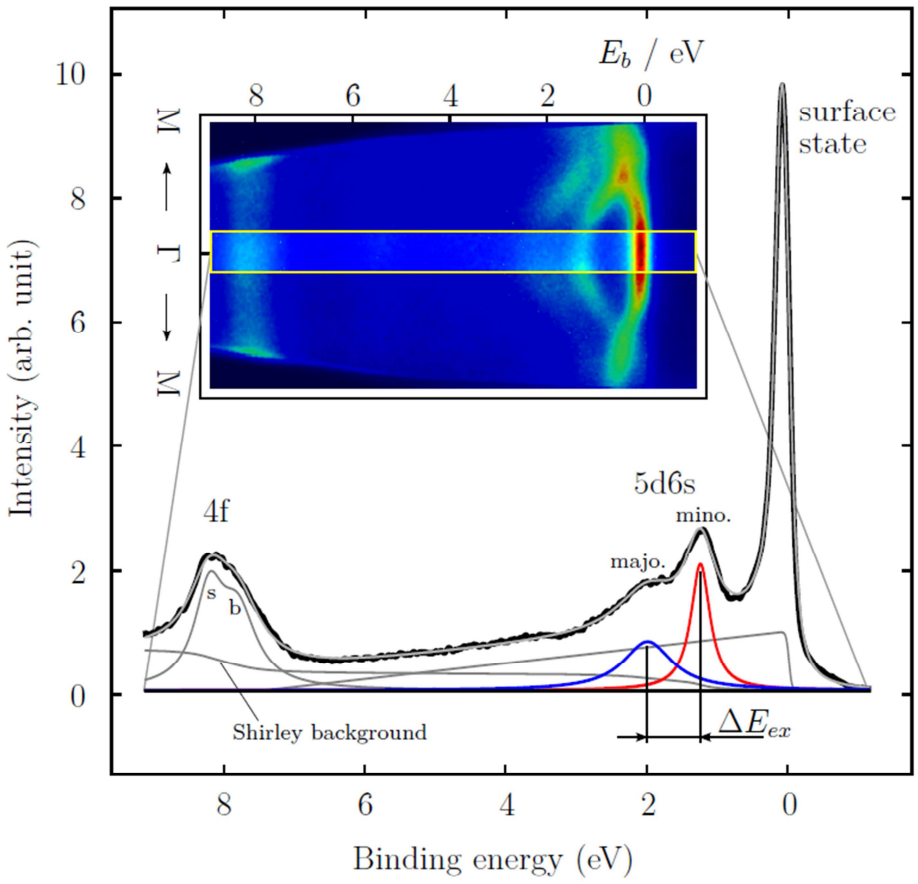

Fig. 1 (Color Online)

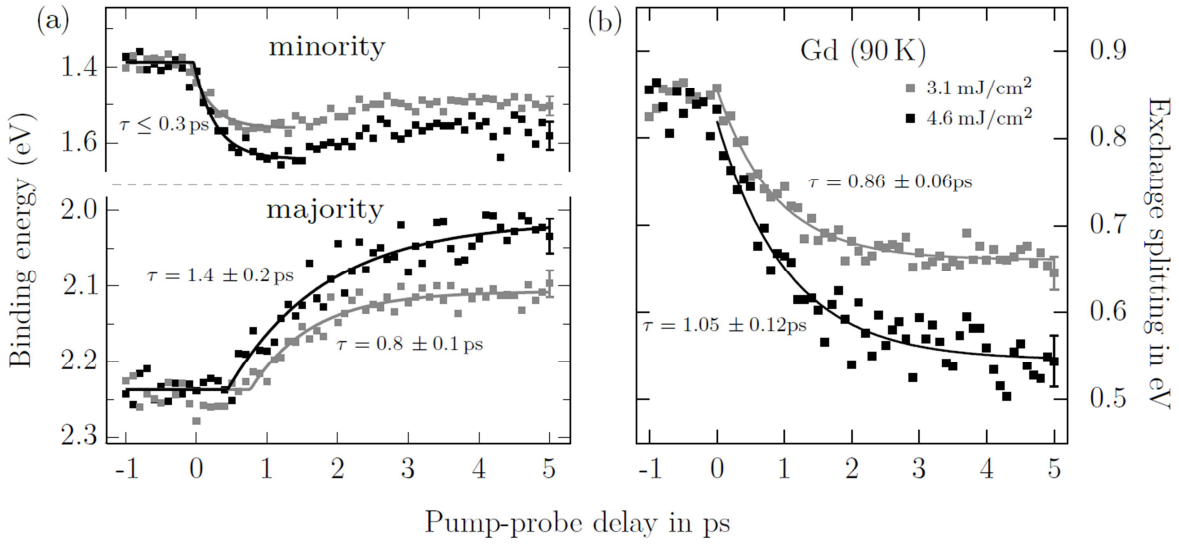

Fig. 2 (Black and white)

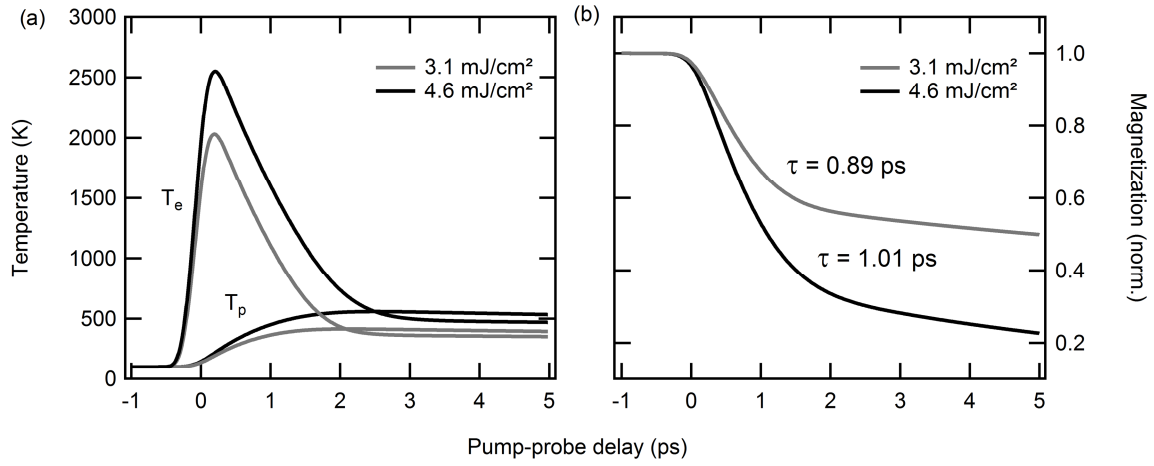

Fig. 3 (Black and white)